Tuning the size and the optical properties of ZnO mesocrystals synthesized under solvothermal conditions

Monica Distaso*; Ruth Wernet; Doris Segets; Wolfgang Peukert

Institute of Particle Technology, Cauerstrasse, 4 - 91058 Erlangen (Germany)
Fax: (+49)913-185-29402 - *E-mail: Monica.Distaso@lfg.uni-erlangen.de

Temperature gradients. It can be expected that in the absence of stirring, especially for large volume, temperature gradients are formed during the reaction. The temperature profile was collected over time by means of three different thermocouples located at different heights (Figure S1 and Scheme 2). A difference of up to 15 °C was found between the bottom of the reactor and the area around the stirrer shaft, due to the fact that the stirrer was joined with the lid and therefore conducted heat inside the vessel. The presence of temperature gradients during the reaction indicates that for large reaction volumes it becomes important to apply stirring in order to ensure a good control over the temperature during the reaction.

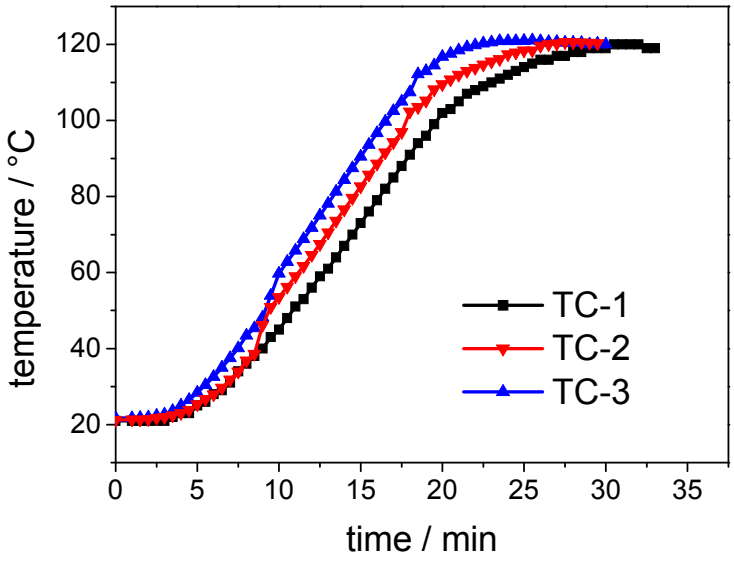

Figure S1. Heating profiles of 300 ml reaction volumes measured at different positions inside the reactor by means of additional thermocouples (TC-1, TC-2 and TC-3) in the absence of stirring (See also technical drawing of the reactor, Scheme 2).

Table T1. Position of the stirrer for different reaction volumes.

Volume, ml	H, cm	h, cm
96	3.1	0.70
150	4.9	1.10
200	6.6	1.50
300	9.8	2.20

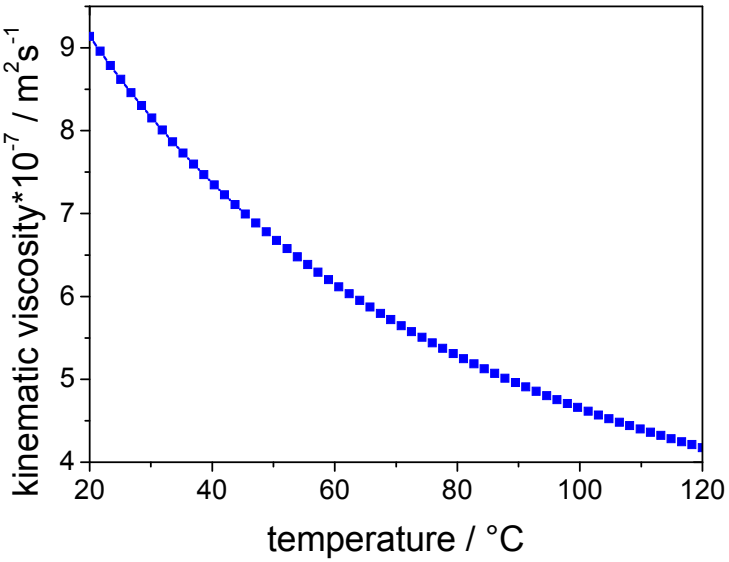

Figure S2. Dependency of DMF viscosity with temperature. The graph was obtained by the simulation program Aspen Plus^{R}.

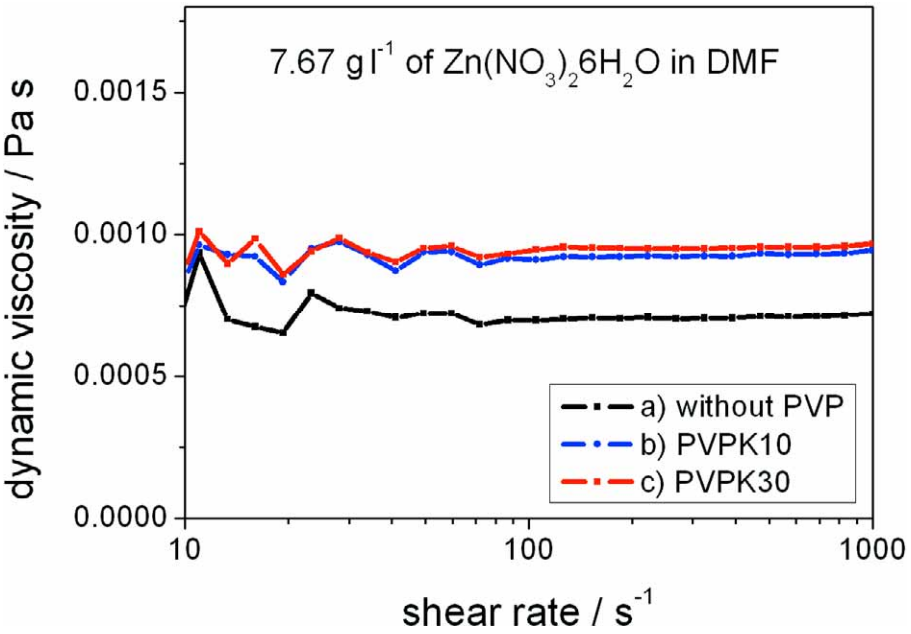

Figure S3: Viscosity as a function of shear stress for different solutions of $Zn(NO_3)_26H_2O$ with and without PVPK10 and PVPK30, respectivelyin DMF. a) only DMF; b) viscosity of a solution of PVPK10 (MW=10,000; 300 mg), $Zn(NO_3)_26H_2O$ (230 mg) in DMF (30 ml); c) viscosity of a solution of PVPK30 (MW=55,000; 300 mg), $Zn(NO_3)_26H_2O$ (230 mg) in DMF

(30 ml). The data show that the presence of Zn Nitrate and PVP increases the viscosity of DMF. However, due to the presence of the same quantity of polymer in terms of mg/ml, the viscosity of the solutions is comparable.

Particle size and size distribution

The $x_{50,0}$ and $x_{50,3}$ can be read from the so-called cumulative distribution $Q_r(x)$. The sub index r indicates the kind of quantity of the distribution, thereby 0 stands for length L^0 (number) and 3 for L^3 (volume, respectively mass).

In order to determine $Q_r(x)$ the total number of particles in the sample has to be determined. Next, the particles have to be allocated into equal intervals of sizes. The mean size of each interval is named x'_i whereas the biggest size of each interval is named x_i. With this information the cumulative distribution can be calculated according to the following equations:

$$Q_r(x) = \frac{\text{number of particles } x \le x_i}{\text{total number}} \qquad \text{(S.1)}$$

In addition the density distribution $q_r(x)$ is also accessible:

$$q_r(x) = \frac{\text{number of particles in the interval between } x_i \text{ and } x_{i+1}}{\text{interval range } (x_{i+1} - x_i) \cdot \text{total number}} \qquad \text{(S.2)}$$

When $Q_r(x)$ and $q_r(x)$ are plotted against particle size, $Q_r(x)$ is correlated to the upper border of interval and $q_r(x)$ to its middle x'_i. The more intervals are introduced, the more accurate the results will be. In Figure S4 and Figure S5 cumulative and density distribution are reported.

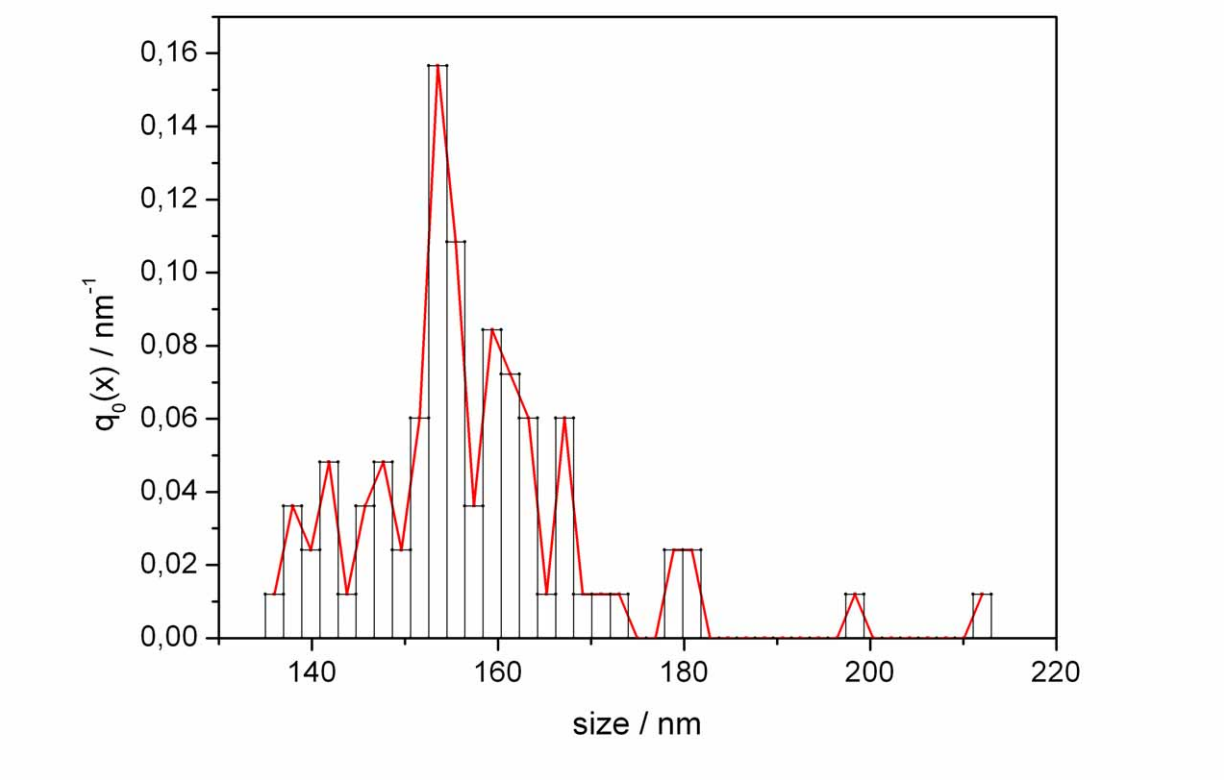

Figure S4. Example of a density distribution.

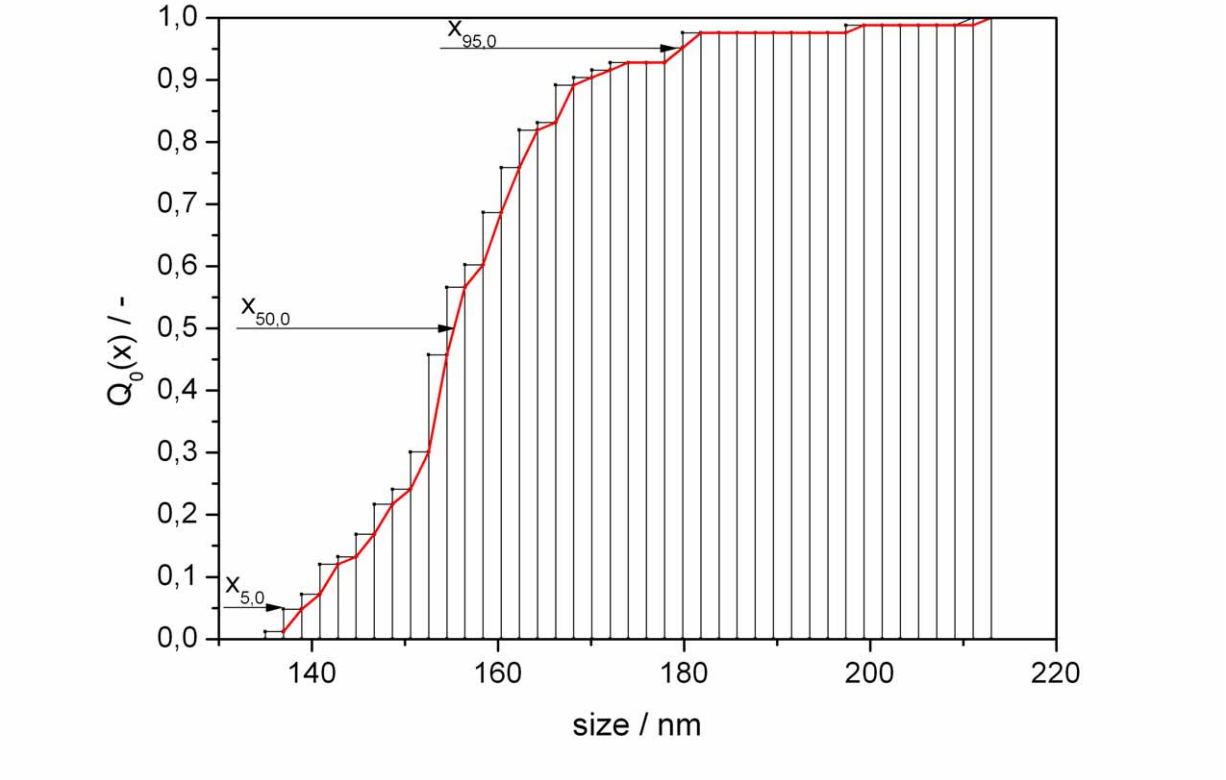

Figure S5. Example of a cumulative distribution.

Table T2. Stirrer velocities in rpm and Re number for each set of energy input experiments performed with different filling level of the reactor.

V, ml	**Energy input, J/ml**	rpm	Re	**Energy input, J/ml**	rpm	Re	**Energy input, J/ml**	rpm	Re
96	**1.27**	329	15200	**0.635**	257	11900	**2.41E-06**	4	200
150	**1.27**	375	17300	**0.635**	298	13740	**2.93E-06**	5	230
200	**1.27**	413	19050	**0.635**	329	15200	**3.71E-06**	6	280
300	**1.27**	473	21800	**0.635**	375	17300	**3.72E-06**	7	320

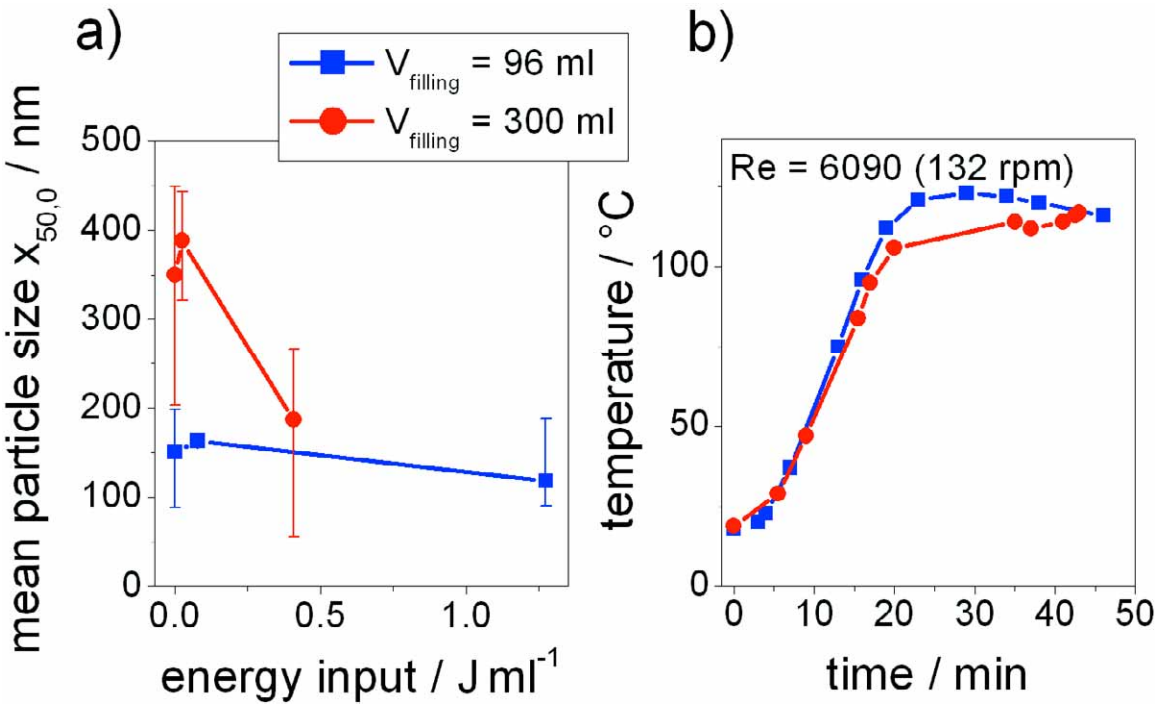

Figure S6. Different energy inputs (a) and temperature profiles (b) for reactions reported in Figure 3 of the paper.

Influence of the width of the PSD to the optical properties. In order to ascertain to what extent the monodispersity of the sample is also able to influence the optical properties of ZnO mesocrystals, the extinction of a bulk 150 nm nanoparticles has been simulated according to Lorenz-Mie theory by using Mie-Plot v 3.4.10 for a monodisperse and for a sample that present a PSD width of ±30 nm. The results show that while the absorption component of the extinction is unaffected by the reduced monodispersity of the sample, the scattering component, and thus the extinction, show a slight deviation, namely a higher scattering

(between 430 nm and 800 nm) when the PSD is narrower. These results also corroborate that not only the size of the particles but also the monodispersity of the sample have to be carefully controlled in order to control the scattering level in the visible region.

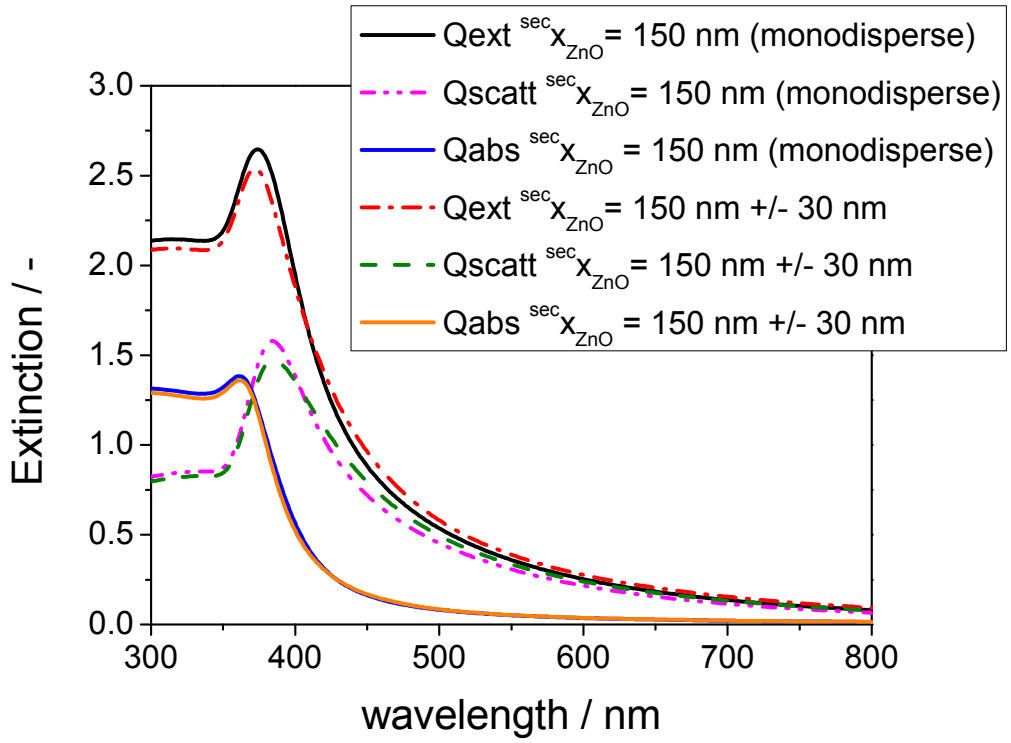

Figure S7. Simulated extinction properties of 150 nm ZnO nanoparticles with a different width of the PSD.

Mechanical stress/strain. Stirring acts on the synthesis of mesocrystals at two levels. The first is a macroscopic one, i.e. mechanical stress and energy are introduced. The second is at the micro- or even at the nano- level and is related to the improved convective mass transfer of building blocks in solution. A mechanical effect of stirring on mesocrystals is also possible, as stirring causes mechanical strain to the particles by promoting impacts on the vessel´s wall or among suspended particles.

In order to ascertain whether the PSDs, standard deviation σ, polydispersity index were affected by the last effect, fully grown and washed particles were re-suspended into pure DMF and treated at high temperature under high stirring rate (657 rpm; Re = 30300) for 2.8 h. It was found that this treatment has no influence neither on the PSD, nor on the width of the

PSD (see Table T6). Therefore, an increase in particle size and consequently the variation of the width of the PSD with stirring rate due to mechanical stress is excluded and stirring mainly affects the synthesis of the particles *during the aggregation step of the reaction*. In principle, this impact can be either destructive (promoting breakage) or constructive (promoting aggregation) but as demonstrated can be neglected.

Table T3. Particles synthesized under solvothermal conditions using 150 ml volume of solution without stirring.

$x_{50,0}$ (no stirring)	$x_{50,0}$ (657 rpm, Re = 30300)
231 nm ±70 nm	226 nm±60 nm

Williamson Hall analysis of the peak broadening.

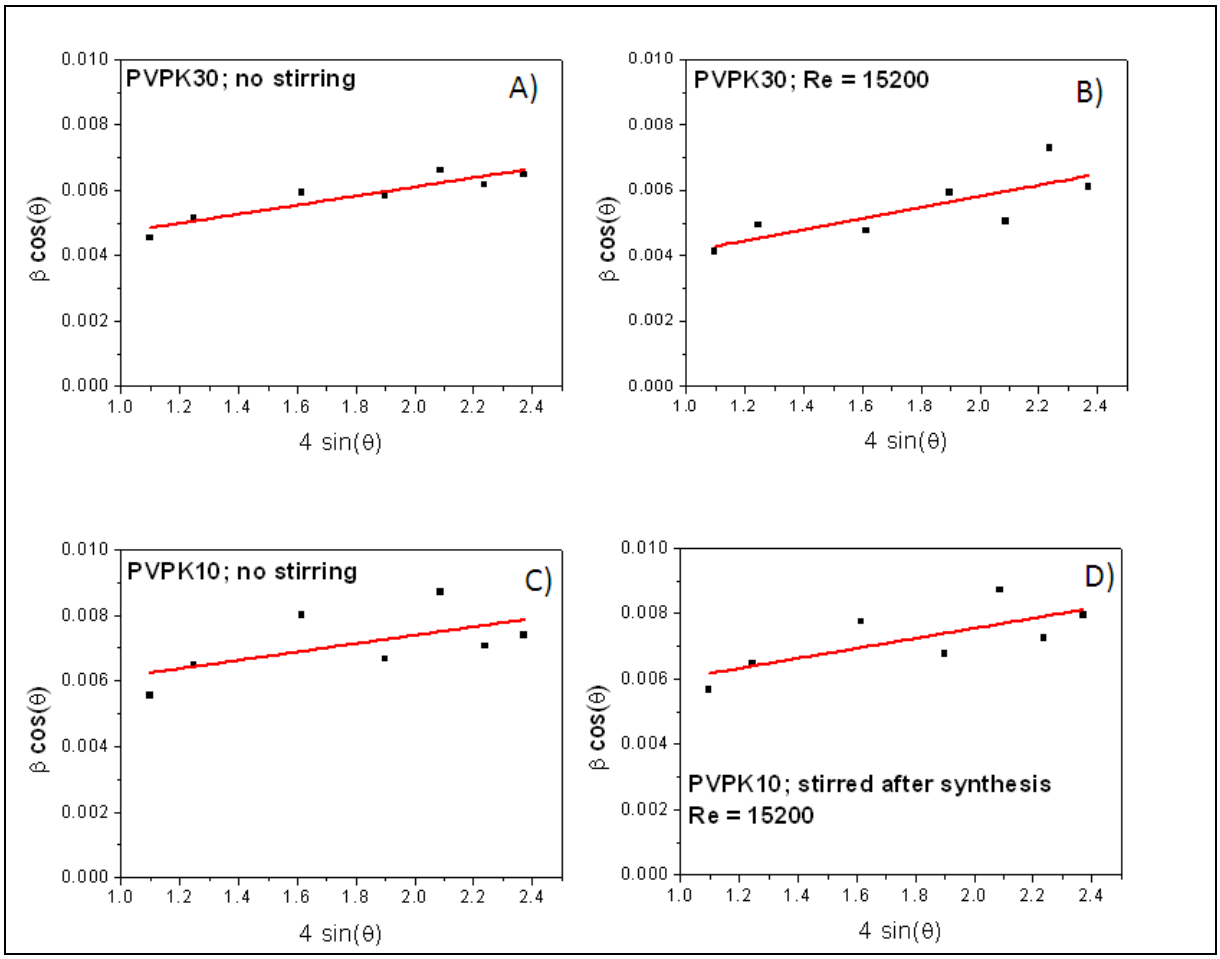

$y = mx + b$

$$D = (K\times\lambda)/b$$

$$\delta D = K\times\lambda\times(-1/b^2)\delta b$$

	$m\times10^{-4}$ (slope)	Standard deviation on m ($\times10^{-4}$)	$b\times10^{-4}$ (intercept)	Standard deviation on b ($\times10^{-4}$)	D±δD
A)	13,9	± 2,56	33,2	±4,73	42 ± 6
B)	16,9	± 6,0	24,2	±10,9	57 ± 26
C)	12,7	±7,5	48,4	±13,9	29 ± 8
D)	15,3	±6,2	44,8	±11,6	31 ± 8

Figure S8 and Table T4. Williamson Hall plot of the samples described in Table 1 (paper): Sample A (Entry 2, Table 1); B (Entry 3, Table1); C (Entry 1, Table 1). Sample D is the Williamson and Hall plot of the particles C, treated under stirring (15200 Re) after being synthesized in the absence of stirring. The analysis demonstrates that the strain is generated during the reaction and cannot be ascribed to a mechanical effect.

As a comparison, the XRD peaks were first refined by applying a Voigt function following a Williamson Hall analysis. In this approach the major reflection (002) was taken into account. The results show that the two approaches lead to comparable final results, both in terms of micro-strain and coherence length, respectively.

In order to ascertain whether the strain was generated by impact of the particles on the reactor wall and on the stirrer blade, ZnO mesocrystals synthesized in the absence of stirring (Entry 2, Table 1, sample C) have been transferred in a DMF volume corresponding to the synthesis volume (300 ml) and heated up to 120°C under a stirring rate of 329 rpm (Re = 15200) and 1.27 J/ml as power input (sample D). The XRD characterization of the particles before and after this treatment demonstrates that the strain was 0.0007 and 0.0008 for the un-stirred and the stirred sample, respectively. Therefore, it was concluded that the strain remained unchanged after the treatment of the particles under stirring. Although the effect observed is very small, any higher strain observed for particles synthesized under stirring has to be due to

misalignment of building blocks and defect formation *during the synthesis, namely during the aggregation step of the reaction*.

Comparison between Williamson Hall and Scherrer Analysis. Due to the presence of strain which also contributes to the broadening of the peaks, the application of Scherrer equation leads to an underestimation of the size of the crystallite, as demonstrated in the following. The broadening of the peaks due to strain increases at higher angles, therefore the crystallite sizes decreases with increases the angle of the reflections and the size calculated according to this method leads to a crystallite size 50% smaller.

Table T5. Results of XRD analysis by applying Scherrer equation to the particles reported in Figure S8_A (PVPK30; no stirring).

	β, (rad)	cos(θ)	$D_v = (K\lambda)/\beta\cos(\theta)$
(100)	0.0047	0.9617	31 nm
(101)	0.0054	0.9502	27 nm
(102)	0.0065	0.9149	23 nm
(110)	0.0066	0.8802	24 nm
(103)	0.0077	0.8529	21 nm
(112)	0.0074	0.8291	22 nm
(004)	0.0080	0.8051	21 nm

Table T6. Results of XRD analysis by applying Scherrer equation to the particles reported in Figure S8_B (PVPK30; Re 15200).

	β, (rad)	cos(θ)	$D_v = (K\lambda)/\beta\cos(\theta)$
(100)	0.0043	0.9617	34 nm
(101)	0.0052	0.9503	28 nm
(102)	0.0052	0.9150	29 nm
(110)	0.0067	0.8804	23 nm

(103)	0.0059	0.8530	27 nm
(112)	0.0088	0.8292	19 nm
(004)	0.0076	0.8059	23 nm

Table T7. Results of XRD analysis by applying Scherrer equation to the particles reported in Figure S8_C (PVPK10, no stirring).

	β, (rad)	cos(θ)	$D_v = (K\lambda)/\beta\cos(\theta)$
(100)	0.0058	0.9616	25 nm
(101)	0.0068	0.9502	21 nm
(102)	0.0087	0.9149	17 nm
(110)	0.0076	0.8801	21 nm
(103)	0.0102	0.8529	16 nm
(112)	0.0085	0.8289	20 nm
(004)	0.0092	0.8050	19 nm

Table T8. Results of XRD analysis by applying Scherrer equation to the particles reported in Figure S8_D (PVPK10, stirred after reaction).

	β, (rad)	cos(θ)	$D_v = (K\lambda)/\beta\cos(\theta)$
(100)	0.0059	0.9617	24 nm
(101)	0.0069	0.9502	21 nm
(102)	0.0085	0.9149	18 nm
(110)	0.0077	0.8802	20 nm
(103)	0.0102	0.8529	16 nm
(112)	0.0087	0.8289	19 nm
(004)	0.0098	0.8055	17 nm

Table T9. Results of XRD analysis by applying Scherrer equation, Williamson Hall and Rietveld refinement to the particles reported in Figure S8 C and D (PVPK10, unstirred and stirred after reaction, Re = 15200).

Sample	Size / **Scherer**	**Williamson Hall** Size Strain	R^2	**Rietveld March-Dollase** Size and strain	Rwp*	**Rietveld Spherical Harmonics** Size / strain	Rwp*
C	21 nm	29±8 (12,7±7,5)×10^-4	0,41	25 nm 8,8% strain	8,62	22 nm 6% strain	6,7
D	21 nm	31±8 (15,3±6,2)×10^-4	0,51	33 nm 12,5% strain	10,94	22 nm 5,2 strain	7,33
*Rwp indicates the goodness of the Rietveld fittig = on a scale from zero to infinity							